ACS APPLIED ENERGY MATERIALS

Article

Photocatalytic Activation and Reduction of CO to CH over Single Phase Nano CuSnS: A Combined Experimental and Theoretical Study

Neha Sharma, Tilak Das, Santosh Kumar, Reshma Bhosale, Mukul Kabir, and Satishchandra Ogale

ACS Appl. Energy Mater., **Just Accepted Manuscript** • DOI: 10.1021/acsaem.9b00813 • Publication Date (Web): 01 Jul 2019

Just Accepted

is published by the American Chemical Society. 1155 Sixteenth Street N.W., Washington, DC 20036

Photocatalytic Activation and Reduction of CO_2 to CH_4 over Single Phase Nano Cu_3SnS_4: A Combined Experimental and Theoretical Study

Neha Sharma,[#,a] Tilak Das,[#,a] Santosh Kumar,[b] Reshma Bhosale[,a] Mukul Kabir [a] and Satishchandra Ogale*[,a]*

[a]Department of Physics and Centre for Energy Science, Indian Institute of Science Education and Research (IISER), Pune, Dr. Homi Bhabha Road, Pune, 411008, India.

[b]Department of Chemical Engineering, University of Bath, Claverton, Bath BA2 7AY, U.K.

KEYWORDS: Photocatalysis, CO_2 reduction, solar fuels, Cu_3SnS_4, Cu-Sn terminated surface.

ABSTRACT

In view of the ability to absorb visible light and high surface catalytic activity, metal sulfides are rapidly emerging as promising candidates for CO_2 photoreduction, scoring over the traditional oxide-based systems. However, their low conversion efficiencies due to serious radiative recombination issues and poor stability restrict their real-life applicability. Enhancing their performance by coupling with other semiconductor based photocatalysts or precious noble metals as co-catalysts makes the process cost intensive. Herein, we report a single-phase ternary sulfide- Cu_3SnS_4 (CTS) as a robust visible light photocatalyst for selective photoreduction of CO_2 to CH_4. It showed remarkable 80 % selectivity for CH_4 evolution with the rate of 14 μmol/g/hr, without addition of any co-catalyst or scavenger. The mechanistic pathway for catalytic activity is elucidated by DFT calculations and *in situ* ATR, which imply formaldehyde pathway of hydrocarbon production. The Cu-Sn termination of the surface is shown to be the key factor for competent CO_2 absorption and activation as confirmed from our X-ray spectroscopy measurements and first principle calculations. This study provides foundation and insights for the rational design of sulfide-based photocatalysts to produce renewable fuel.

1. INTRODUCTION

Over usage of fossil fuels to meet the ever-increasing electricity demand has led to excessive anthropogenic CO_2 emissions in the environment resulting in several harmful consequences; global warming being the most alarming amongst all. Inspired by the natural photosynthesis process by plants, CO_2 reduction using photon energy from the sun and an active photocatalyst is considered as an attractive approach in this context, as it produces storable renewable fuel, and at the same time, mitigates the greenhouse gas emission.[1,2,3,4]

The foremost and fundamental step in photocatalytic CO_2 reduction is the absorption of CO_2 on the surface of a photocatalyst. Besides adsorption, CO_2 activation and further reduction to value-added products are also the other two crucial steps for the completion of photocatalytic reaction efficiently. However, CO_2 is a highly stable and chemically inert molecule with linear geometry. Thermodynamically stable CO_2 molecule requires large Gibbs free energy (~393.5 kJ/mol. at 298 K) for bending and breaking of the C-O bonds.[5,6] More specifically, the reduction of CO_2 in the presence of H_2O into hydrocarbon fuel such as CH_4 and CH_3OH is a multistep multi-electron-proton-coupled uphill reaction with a higher positive change in the Gibbs free energy of 818.3 kJ/mol and 702.2 kJ/mol, respectively. This makes the CO_2 reduction a grand challenge to the researchers.[5,7] To overcome the difficulties in this current scenario, detailed investigations of highly active and selective photocatalytic systems and their surfaces, combining experimental and theoretical insights, are extremely essential.

Since Inoue and co-workers[8] reported their pioneering work on the photocatalytic CO_2 reduction over TiO_2, many such class of materials like metal oxides (ZnO,[9,10] TiO_2,[11,12] Ga_2O_3 [13,14]), metal sulfides (CdS[8,15,16] Bi_2S_3,[17] ZnS,[18] Cu_2S[19], SnS_2[20,21]), phosphides (GaP)[8], and Nitrides (C_3N_4[22,23]) have been studied in this context. Among them, the most popular choice of a photocatalyst is TiO_2

due to its low cost, high stability and non-toxicity. However, its relatively wide band-gap (~3.1-3.3 eV) and UV responsive nature (forms only about 4% of solar spectrum) seriously restrict its solar conversion efficiency.[12] Among the visible light active photocatalysts reported so far, metal-sulfides are considered as excellent candidates for their high optical absorption in the visible region of the solar spectrum because of their narrow band gap and high catalytic activity.[24] In particular, binary sulfide CdS is well studied as an effective visible light photocatalyst with a narrow band gap of 2.4 eV along with favorable conduction band positioning of CdS.[8] However, several technical issues limit the photo-assisted redox activities of CdS such as aggregation of CdS nanoparticles resulting in decrease in the effective surface area, photo-instability and photocorrosion, and consequently high rate of electron hole pair recombination[15,16]. Among the ternary sulfides very few materials have yet been studied such as $CuInS_2$ which showed selective CH_4 production at 2.5 μmol/g/hr after coupling with TiO_2.[25] Kudo *et al* [26] demonstrated $CuGaS_2$ as an efficient photocatalyst with a series of sulfide materials coupled with RGO-TiO_2 delivering 0.25 μmol/g/hr of CO gas. Most of them are either coupled with semiconductor or co-catalyst such as Pt to boost the performance but the current state-of-art requires much more improvement in the performance features. Nevertheless, stand-alone (without scavenger/co-catalyst/noble metal coupling) ternary sulfides for photocatalytic CO_2 reduction are till date unexplored. Moreover, explicit understanding of pristine surface of photocatalyst and CO_2 interaction over the sulfide surface is also still lacking.[27]

Herein, we report for the first time a single-phase ternary metal sulfide Cu_3SnS_4 (CTS) as a highly stable stand-alone visible light photocatalyst for CO_2 reduction into C1 hydrocarbons. Although CTS is explored for the applications of solar cell and dye/pollutant degradation, to the best of our knowledge there is no report on its application for photocatalytic CO_2 reduction.[28–30] In the gas

phase, photocatalytic CO_2 reduction over our pristine CTS delivered CH_4 as a major product with 80% selectivity (without the addition of any co-catalyst or scavenger) at the rate of 14 μmol/g/hr. Apart from the excellent photocatalytic activity, CTS also displayed very good photostability for more than 17 hrs. Experimentally, CTS showed its thermodynamic viability to reduce CO_2 to C1 hydrocarbon due to appropriate alignment of energy levels with respect to reduction potentials of CO_2. Besides, our density functional theory (DFT) calculations reveals that CTS has an explicit Cu-Sn terminated (001) surface which is extremely competent to promote CO_2 absorption as well as deformation. Additionally, *in situ* ATR could elucidate the genesis of intermediate species and reaction mechanism in photocatalytic CO_2 reduction over CTS. Over all, our results highlight that bivalency of Copper i.e. Cu^{1+} or Cu^{2+} on the CTS surface plays a very crucial role in the CH_4 production through formate intermediates following the formaldehyde pathway. As per our knowledge, this is the first report on ternary sulfide CTS (without a co-catalyst or scavenger) for CO_2 photo-reduction analyzed via combined experimental and theoretical approach.

2. EXPERIMENTAL SECTION

2.1. Material Synthesis

The Cu_3SnS_4 nanoparticles were synthesized as given in our earlier report.[31] Briefly, the metal precursors, namely copper acetylacetonate and tin chloride were taken in certain molar ratio with excess of thioacetamide as the sulfur precursor. The reagents were taken in a three neck vessel with formamide as the solvent and were degassed under nitrogen for half an hour with constant stirring. Then, the mixture was heated to 170 °C at a rate of 10 °C/min and kept at that temperature for one hour. After completion, the reaction was quenched to room temperature. The nanoparticles were obtained by centrifuging and washing with ethanol several times. The NPs were dried at 80 °C overnight.

2.2. Characterization

Material Characterization: To confirm the crystal structure of CTS powder X-Ray diffraction (XRD) was done using Bruker D8-Advance X-ray Diffractometer (Germany) with Cu kα (wavelength = 1.5418 Å). The Raman study was performed using LABRAM HR 800 from Jobin Yvon Horiba. Morphology of CTS samples were studied by scanning electron microscopy (SEM) which was done using FEI Nova Nano 450 SEM. The High-resolution transmission electron (TEM) microscopy was performed with FEI, Tecnai F30, and FEG system with 300 kV. The Brunauer-Emmett- Teller (BET) adsorption measurements for surface area calculation were done using Quadrasorb automatic volumetric instrument. X-ray Photoelectron Spectroscopy (XPS) study was performed using a PHI 5000 Versa Probe II equipped with a mono-chromatic Al Ka (1486.6 eV), a X-ray source and a hemispherical analyzer. Valence band XPS was performed ona Kratos Axis HSi spectrometer with a monochromated Al Kα X-ray source operated at 90 W and magnetic charge neutral-izer. The Ultraviolet-Visible diffuse reflectance spectrum (UV−VIS DRS) was obtained by SHIMADZU UV-3600 plus UV-VIS-NIR spectrophotometer with integrating sphere attachment. In situ ATR Infrared spectra were recorded on a Thermo Nicolet FT-IR spectrometer, equipped with a liquid nitrogen cooled MCT (mercury cadmium telluride) detector and an external attachment for ATR-IR measurements. The ATR crystal for a gas flow-through cell is made of ZnSe with 45° reflection crystal.

Electrochemical Measurements

Mott-Schottky plot was obtained by performing the measurements in three-electrode system using AUTOLAB PGSTAT 30 potentiostat. In three-electrode system, Ag/AgCl was used as reference electrode, Platinium as counter electrode, and sample coated on Fluorine doped Tin oxide (FTO) as the working electrode. The measurements were carried out in 0.5 M Na_2SO_3 electrolyte. The

photoelectrodes were fabricated by preparing the slurry in mortar pistil by adding 40 mg sample, 200 ul Nafion (5%) and 1ml iso-propanol (IPA). The obtained paste was coated on FTO with 1cm^2 area and heated at 250°C for 1hr to get homogenous film. Mott Schottky plots were recorded in dark at the scan rate of 10 mV/s with the frequency of 10 KHz. HER plots were obtained in a three electrode system with glassy carbon electrode (GCE) as the working electrode by using CH instruments.

Photocatalytic measurements

Gas phase photocatalytic CO_2 reduction experiments were carried out in a setup made of stainless-steel photoreactor with quartz window, under the illumination of solar simulator (100 mW/cm^2) equipped with Xenon lamp. Prior to irradiation the reaction set up is vacuum treated, purged with He (20 ml/min for 1 hr) to remove the internal air and purged with high purity CO_2 for 1 hr along with water vapour. During irradiation 1ml of gaseous product from the setup is sampled and subsequent analysis was done by Gas Chromatography (Shimadzu Tracera GC-2010 Plus) with Barrier Ionization Detector (BID) and He carrier gas. Liquid products were also analysed periodically from separate aliquots on an Agilent 1260HPLC fitted with a Hi Plex column, however only traces of methanol detected in this study. For stability test, CTS sample was collected after each run, refreshed by washing with water and its performance was re-evaluated by the aforementioned procedure. The Selectivity of formed CO was deduced according to the following equation:

$$\% \text{ of } CH_4 \text{ selectivity} = \frac{8N_{CH4}}{8N_{CH4} + 2N_{CO} + 2N_{H2}} \times 100$$

In which, $N_{CH4,}$ N_{CO} and N_{H2} stand for the yield of reactively formed CH_4, CO and H_2, respectively.

$$\% \text{ of CO selectivity} = \frac{2N_{CO}}{8N_{CH4} + 2N_{CO} + 2N_{H2}} \times 100$$

In which, N_{CO} and N_{H2} stand for the yield of reactively formed CO and H_2, respectively.

Apparent quantum yield (AQY) of the photocatalyst was calculated using the following equation:

$$\text{AQY } \% = \frac{\text{The number of evolved CH4 molecules} \times 8}{\text{The number of incident photons}} \times 100$$

3. RESULTS AND DISCUSSION

Phase purity of the orthorhombic Cu_3SnS_4 nanoparticles was confirmed by X-ray diffraction (XRD) as reported earlier and is shown in Figure S14 (a).[31] Morphological and microstructural features were also studied by FESEM and TEM techniques and the corresponding images are given in the Supporting Information Figure S14. These reveal that the size of CTS nanoparticles is about 5 nm. The positive slope in Mott-Schottky plot as given in the inset of **Figure 1a** indicates n-type conductivity of CTS. To evaluate the thermodynamic feasibility of CTS in the targeted application context, band levels were estimated from the band-gap and Valence Band (VB) spectroscopies. The Tauc plot (Supporting information S1) derived from the DRS depicts the optical band gap of 1.76 eV, implying CTS as a visible light photocatalyst. The measured VB edge of CTS (**Figure 1a)** is 0.64 eV. Hence, the CB (conduction band) for CTS from the band-gap is calculated to be -1.12 eV vs. NHE. Thus, with the obtained values for CB and VB of CTS, it is possible to derive a schematic energy level diagram with respect to reduction potentials of CO_2 to different reduced products as given in **Figure 1b**. It clearly indicates that in CTS the CB edge has much more negative potential relative to required reduction potential of CO_2 to get reduced products and it is indeed a thermodynamically viable visible light-driven photocatalyst. We also performed DFT calculations with Van der Waals dispersion energy corrections (at D3 level) [32,33] to study the surface of CTS.[31] Since (001) is the preferred orientation obtained from the XRD, we have

performed all the DFT calculations on the same surface. It is demonstrated that (001) surface of CTS is Cu-Sn terminated with sublayer of S atom as shown in the schematic (**Figure 2b)**.

Photocatalytic CO_2 Reduction over CTS (001) surface

Experimentally, after 5 hrs of gas phase photoreduction of CO_2 on CTS sample CH_4 ~ (71 μmol/g), CO ~ (42 μmol/g) and H_2 ~ (31 μmol/g) were obtained as resultant reduced products, as shown in **Figure 1c**. Trace amount of CH_3OH was also detected by HPLC. O_2 evolution ~ (178 μmol/g) was the oxidised product from water oxidation reaction (discussed in details in Supporting Information S2 a). The total volume of the O_2 produced was correlated with the total volume of reduced products which indicate that $(CO+H_2)$: O_2 and CH_4 : O_2 ratio is in the stoichiometric ratio of 2:1 and 1:2, respectively, which indicates that water is consumed as a reducing agent (electron donor) in the overall reaction. The control experiment (Supporting Information S2 b) indicates that almost no CO or hydrocarbon is detected in the absence of either the photocatalyst or light, suggesting that the obtained reduced products are the result of the photocatalytic reaction on the surface of the photocatalyst. Secondly, in the absence of the CO_2 gas, no products were evolved indicating unequivocally that the carbon source of reduced products (CO and CH_4) is from CO_2 and not from any other source. Among the obtained products, CH_4 was produced as a major product with 80% selectivity at the rate of 14 μmol/g/h without addition of any co-catalyst or scavenger agent. Moreover, reusability of CTS evaluated by successive 3 cyclic runs for 17 hrs of light illumination (**Figure 1d**) could be clearly established and signifies that CTS surface has very good stability for longer run experiments. The same is shown in the form of histograms with three repetitions for CH_4, CO and H_2 in Figure S15 of SI.

X-ray Photoelectron Spectroscopy (XPS) Analysis of CTS (001) Surface

The step of CO_2 adsorption is not only the necessity but also the foundation towards increasing the CO_2 uptake and photoactivity of a solid photocatalyst. To gain the insights into the exact mechanism and the role of Cu exposed CTS surface experimentally as well as theoretically, XPS data was analysed as given in **Figure 2**.

The Cu 2p spectrum display two peaks positioned at $2p_{3/2}$ (932.3 eV) and $2p_{1/2}$ (952.1 eV), which is deconvoluted into doublets. This indicates the presence of Cu^{1+} and Cu^{2+} on the CTS NPs surface.[34,35,36] The concentration of Cu^{1+} on the surface of CTS is more as compared to Cu^{2+} which is in agreement with DFT prediction (details in Supporting Information S3). From our calculations using PBE-GGA functional of the core levels of Cu ions using the core-hole approach as implemented in Wien2K code[37] showed results for the L_2 edges of the two types of Cu atoms (~948 eV) indicating existence of copper in both Cu^{1+} and Cu^{2+} on the surface of CTS in accordance with experimental interpretation from XPS. However, the exact stoichiometric amount of the Cu^{1+} and Cu^{2+} in the slab cannot be predicted from the present ground state first-principles core-hole calculations. The details of experimentally measured Sn and S XPS results are given in Figure S3. Thus, the surface edge with Cu-Sn termination represents the most available active sites for the catalytic reactions, supported by sub-layer of S atoms in a pristine CTS (001) surface. Therefore, over the Cu-Sn terminated (001) surface of CTS interaction of CO_2 and H_2O molecules was studied by DFT+D3 level as to probe the mechanism of CO_2 reduction.

Mechanism of H_2O Breaking and CO_2 Activation from DFT Prediction

As the activation of the CO_2 molecule is highly assisted in the presence of water vapour under the present experimental conditions, adsorption process of the H_2O molecule over the CTS surface

was examined preliminarily from our first-principles DFT+D3 theoretical calculations (Supporting Information S4 and Table S1). Herein, we considered only three possibilities for H_2O adsorption due to the polar and more electronegative character of the H_2O, which can be a best fitted to the three available metal sites on the CTS surface. (Details are in Supporting Information S5). Out of these three types of metal sites, only Cu^{1+} or Cu^{2+} sites are highly favourable for the H_2O physisorption with calculated binding energies -0.2 eV whereas the Sn-site does not accept the H_2O due to positive binding energy. The measured <H-O-H> angle is ~106.5° after the optimization of the atomic positions using DFT+D3 level functional, which led to out-of-plane distances of ~0.227 and 0.224 nm from Cu^{1+} and Cu^{2+} sites of CTS (001) surface, respectively. Indeed, the calculated Fermi level is up-shifted due to H_2O adsorption at Cu sites by ~0.15 eV than the pure CTS surface from our calculations, which is also another signature of weak physisorption of H_2O over the CTS surface (H_2O@CTS).

Similarly, the calculated binding energies of the different possible models of the isolated CO_2 over the Sn-Cu terminated (001) surface of the CTS are shown in the Table S1 of SI. We note a clear indication that isolated CO_2 can be physisorbed as the values of E_b are within few tens to few hundreds of meV per mole. Out of all the models, the best preferred site for the CO_2 is the hollow site enclosed by Cu^{1+}-Cu^{2+}-Cu^{1+} triangle with linear CO_2 perpendicular to the Cu^{1+}- Cu^{1+} chain, with calculated binding energy of -0.660 eV per molecule of CO_2 (Supporting Information S6 in Model [b] and Table S1), followed by the three models i.e. i) model [a] with O-atom of CO_2 over the Cu^{1+} of the CTS and perpendicular to the Cu^{1+}- Cu^{1+} chain with binding energies -0.135 eV, and ii) model [f] the next model with CO_2 within the hollow hexagon formed by Cu^{1+}-Sn^{4+}-Cu^{2+} triangle unit and parallel to Cu^{1+}-Cu^{2+} chain with binding energies -0.115 eV, and finally iii) model [d] the model with the CO_2 is perpendicular to the Cu^{1+}-Cu^{2+} chain, with calculated binding

energies -0.107 eV. We observed that in all these four models, the optimized CO_2 molecule remained linear and no activation (bending) is observed with calculated angles of CO_2 i.e. <O-C-O> are 179.5°, 179.7°, 179.6°, and 179.7°, respectively.

The current state-of-art of solo CO_2 adsorption scenario changes dramatically, once we combine best preferred sites for both the molecules, CO_2 and H_2O, over the CTS NPs (001) surface during computer modelling. Thus, we have proceeded with total four possible models by combination of these previously mentioned four models of CO_2@CTS and two models of H_2O@CTS to validate the route of CO_2 reduction (Details are in Supporting Information S7 of SI). The first step of the CO_2 reduction is single proton and two electron transfer, as given in the following equation[38],

$$CO_2 + H^+ + 2e^- = HCOO^- \text{ at } E_0 = -0.49V \text{ vs. NHE.} \quad (1)$$

Similar kind of phenomena is observed in one of our proposed four models combining the CO_2 and H_2O with CTS from first-principles calculations with optimized hybrid geometry shown in **Figure 3a**, where only the specific projection of the 2×2 super cell structure is shown for better visualization. It is clear from the figure that the combined model CO_2@CTS with the H_2O@CTS best suits complete distortion of the CO_2 into OH^- and $HCOO^-$ via bending of CO_2 with angle ~123° which is reasonable with the required CO_2 activation angle of ~120°-140°. Both the Cu sites are preferred to the H_2O adsorption, but thermodynamically the Cu^{2+} site is helpful in breaking of H_2O due to unfilled d orbital i.e. $3d^9$ by trapping the photo generated electrons. Consequently, Cu (II) gets converted to Cu (I) and trapped electrons are utilized in radical formation. The formed Cu (I) could be reoxidised to Cu (II) by protons from the system as given in equation (2) and (3). Such a sequential reaction reduces the rate of electron hole recombination increasing the selectivity and yield of reduced products.[39]

$$Cu\ (II) + e^- \rightarrow Cu\ (I) \quad (2)$$

$$Cu\ (I) + H^{+} \rightarrow Cu\ (II) \qquad (3)$$

Hence, the accessibility of valency switching of Cu at the CTS surface plays an important cyclic oxidation and reduction of H_2O, respectively with constant generation of protons which is the key necessity for continuation and completion of CO_2 reduction. Such changes in valency mediated via the presence of native defect sites cannot be excluded; indeed, affecting overall changes of the charge state of Sn sites from Sn^{4+} to Sn^{2+}. More number of Cu^{1+} sites, are helpful to separate the protons and their radicals from rapid recombination as a donor, whereas the Cu^{2+} as an acceptor enhances the format redox route.

In **Figure 3b**, we have sketched one schematic following our first-principles calculated optimized geometry of the CTS (001) slab combining with H_2O and CO_2.This is in accordance with our XPS observation of the two types of Sn sites present on pristine CTS surface. Once protons are available at the Cu^{2+} site, in the presence of CO_2 and photon the formation of $HCOO^{-}$ is feasible on the CTS surface as we observed from our DFT+D3 optimized structure analysis. One of the bond lengths of C-O is slightly larger (1.29 Å) than the far most C-O bond length (1.24Å), with Cu^{2+}-O distance ~ 2.3Å which are favourable conditions for the CO_2 activation; those have been fulfilled here. Hence, the possible pathway of CO_2 photoreduction over CTS proceeds through formaldehyde way. The other three possible models of combined with CO_2@CTS and H_2O@CTS, respectively, remain a weak physisorption process and can be ruled out in this present discussion (Details are in Supporting Information S7). To confirm the formaldehyde pathway experimentally *in situ* ATR was conducted over CTS surface.

In situ ATR Analysis for the Mechanism of Photocatalytic CO_2 Reduction

To detect the intermediate products and to obtain further insights into the mechanism of photocatalytic CO_2 reduction over CTS, *in situ* ATR measurements were conducted (Results in

Figure 4). IR of CTS purged with CO_2 gas and water vapour was recorded in dark and under light illumination for 30 mins and later for 60 mins to study the reaction sequence by ATR. In photocatalytic CO_2 reduction, when light is incident on the photocatalyst, electron-hole pair is generated and the photogenerated carriers migrates to the surface. The photogenerated electrons from the CB of the photocatalyst along with protons from H_2O reduce CO_2, as the photocatalyst has much more negative potential than the reduction potential of CO_2; while the holes from VB of the photocatalyst does oxidation of water to produce O_2. The resultant reduced products finally get desorbed from the surface. In the dark, combination bands of molecular CO_2 around (3500-3700 cm^{-1}) and molecular H_2O (2900-3500 cm^{-1}) from purged CO_2 and H_2O are observed.[40] Apart from molecular gas small vibration peaks of asymmetric stretching of CO_2 (2150-2200 cm^{-1}) and bending vibrations of –OH groups (1630-1640 cm^{-1}) are observed, indicating the interaction of these gases with CTS surface even in dark.[40,41] More surprisingly, a weak peak at 1264 cm^{-1} is observed indicating the presence of $CO^{\bullet}_2$.[41,42] Existence of $CO^{\bullet}_2$ radical as an intermediate species during the photoreduction of CO_2 by capturing the electron from the conduction of catalyst is a controversial issue due to its thermodynamic barrier.[5] Additionally, its rapid conversion into further intermediates and product makes its detection difficult. Even many theoretical and experimental research groups have verified the $CO^{\bullet}_2$ species by different configuration.[41,42,43,44] In our case also we observed bending of CO_2 on the Cu-Sn terminated (001) surface of CTS by DFT+D3 computation of geometry (Figure 3a). $CO^{\bullet}_2$ adsorbate has a bent configuration and lower barrier to accept electrons for further activation of CO_2 as compared to the linear free CO_2 molecule.[5]

After light illumination, appearance of two new distinct broad bands at around 1200-1400 cm^{-1} and 1550-1650 cm^{-1} were clearly seen. The mode at around 1660 cm^{-1} is characteristic of bidentate

carbonate b-CO_3^{2-} which indicates that CO_2 molecule is bonded to CTS surface through its oxygen rather than by carbon,[5,42] which is well corroborated with interpretation from our DFT (S2 in Supporting Information).The bands at 1460 and 1621 cm^{-1} correspond to bicarbonate species HCO_3 which arises from the reaction of absorbed CO_2 and surface hydroxyls from dissociative H_2O molecule.[42] Two sharp bands at around 2160 and 2200 cm^{-1} represent the asymmetric vibrations of CO_2 or CO bonded with Cu (I) and Cu (II),respectively.[45,46] The existence of Cu^{1+} and Cu^{2+} on the surface of CTS is also confirmed experimentally (XPS) and theoretically (DFT) in our case which is in agreement with the ATR results. Such bands indicate that the Cu terminated surface has important role to play for providing absorption site for CO_2 and for its deformation. Importantly, a new and broad band at around 1360 cm^{-1} is observed which is attributed to asymmetric stretching of OCO arising from bidentate HCOO*. Formation of this species indicates that the photocatalytic mechanism may have proceeded through formaldehyde pathway by formation of bidentate formate as an intermediate species which finally leads to CH_4.[42,47,48]

$$CO_2 \rightarrow HCOOH \rightarrow H_2CO \rightarrow CH_3OH \rightarrow CH_4 \quad (4)$$

Thermodynamically this is possible in the CTS case, as it has negative conduction band (-1.1 V vs NHE) compared to the reduction potential of CO_2 to HCOOH (-0.61V vs NHE) by transfer of two electrons.[5] We also observed trace amount of methanol as a reduced product under the gas phase of experimental conditions, which perhaps must have got consumed further for the formation of CH_4 as per the equation (4). In addition, formate can reoxidize itself to produce CO. The very weak bands at around 1112 cm^{-1} and 3019 cm^{-1} are characteristics peaks of CO and CH_4, respectively [48,49], which are an indication that formation of target products is initiated after the 30 mins of light illumination by the reaction of intermediate photoactive species: b-CO_3^2, HCO_3^-, OCO, OH- by H_2 as reductant. Further, 60 mins of illumination showed increase in the peak

intensity of CO and CH_4 with subsequent reduction of b-CO_3^{2-}, HCO_3^-, OCO. Also, generation of a new distinct peak corresponding to C-H bending from C1 hydrocarbons is also observed at 1390 cm^{-1}.[49,50] Combining our results based on the spectral changes it can be speculated that $CO^{\bullet}_2$ and OCO are deemed to be the key intermediates for formation of bidentate formate which is utilized for the production of CH_4. Based on ATR results and formed products the possible mechanism can be elucidated by following equations:[5,42,48,51,52]

$CTS + h\nu = CTS\ (h^+_{VB} + e^-_{CB})$

$2H_2O + 4h^+ = 4H^+ + O_2 \quad (E^0 = +0.82\ V)$

$CO_2 + e^- = CO_2^{\bullet -} \quad (E^0 = -1.90\ V)$

$CO_2 + 2H^+ + 2e^- = CO + H_2O \quad (E^0 = -0.53\ V)$

$CO_2 + 4OH^- = CO_3^{2-} + 2H_2$

$CO_3^{2-} + OH^- = HCO_3^- + 2O_2$

$CO_2 + 2H^+ + 2e^- = HCOOH \quad (E^0 = -0.61V)$

$CO_2 + 8H^+ + 8e^- = CH_4 + 2H_2O \quad (E^0 = -0.24\ V)$

$CO_2 + 6H^+ + 6e^- = CH_3OH + H_2O \quad (E^0 = -0.38\ V)$

$2H^+ + 2e^- = H_2 \quad (E^0 = -0.41\ V)$

Still the question remains as to how and why eight electrons and eight protons coupled process of particular CH_4 production is so favoured over the Cu-Sn surface as compared to other resultant reduced products of photo-reduction of CO_2. Firstly, Cu ions can act as an active centre for CO_2 photoreduction as they can trap the photo-generated electrons from the CTS surface due to unfilled

d-orbital, thereby inhibiting electron hole recombination.[42,45,46] Consequently, more number of photo generated electrons are available for activation of CO_2 and for the genesis of intermediate products, and ultimately should increase the quantum yield of photocatalyst. In our case as well, the obtained Apparent Quantum Yield (AQY) for CTS is 1.63% which is higher than the earlier reported values.[53,54,55,56] Secondly, Cu not only participates in the activation of CO_2 but it also suppresses the simultaneously occurring undesirable HER reaction which ultimately increases CH_4 selectivity and yield as accumulated charges on the surface is well utilized in CO_2 reduction.[57,58]

To confirm the above, we also performed the electrochemical experiment to evaluate the HER activity of CTS in the presence of Ar and CO_2 both as given in Supporting Information S8 which clearly indicates that the Cu terminated CTS surface has more affinity for CO coverage, which weakens the binding of hydrogen on surface to produce H_2. It is difficult to compare the CO_2 reduction yield of products over CTS with other sulfides due to different experimental conditions but we have given a Table S2 of the comparison (Supporting information) where CTS stands at the top without any addition of co-catalyst of scavenger. In conclusion, Cu ion increases the probability of electrons transfer to adsorbed CO_2 and for the genesis of intermediate reactive species like $CO^{\cdot}_2$ formate $HCOO^-$, which eventually forms C1 or higher hydrocarbons. The formation of CH_4 from the formaldehyde pathway proceeds through the formation of formate, which is stabililized by the valence of Cu.

Conclusion

The present work demonstrates that single-phase ternary sulphide Cu_3SnS_4 nano-particulates as an efficient visible light photocatalyst for selective CO_2 reduction to CH_4. It shows an excellent photocatalytic performance of 71μmol/g of CH_4 with good selectivity and stability. We attempted to elucidate the mechanism by investigating and studying the pristine surface of CTS and

interaction of CO_2 over it. Our DFT+D3 predictions indicate that CTS possesses Cu-Sn terminated (001) surface which promotes CO_2 adsorption and activation. To summarize, from our experimental and theoretical calculations we conclude that Cu-Sn terminated CTS follows formaldehyde pathway for production of C1 hydrocarbon. The present work provides the foundation for the rational design of sulfide based photocatalyst to produce renewable fuel.

ASSOCIATED CONTENT

Supporting Information: Tauc plot, control experiment of photocatalytic CO_2 reduction, O_2 evolution data. Detail theoretical study of interaction of CO_2 and water vapour over CTS by DFT, HER plot and table of comparison of different catalyst with CTS.

AUTHOR INFORMATION

***Corresponding Authors**

E-mail: reshmabhosale10@gmail.com

E-mail: satishogale@gmail.com, satishogale@iiserpune.ac.in

Author Contributions

The manuscript was written through contributions of all authors. All authors approve the final version of the manuscript. # Neha Sharma and # Tilak Das have contributed equally.

Notes

Authors declare no competing financial interest.

ACKNOWLEDGEMENT

Authors would like to thank DST Nanomission (Thematic Unit SR/NM/TP-13/2016), Govt. of India and the UK-India SUNRISE (GCRF) Grant for research funding. SK also thanks the

Engineering and Physical Sciences Research Council (EPSRC) (EP/R035407/1) for financial support. SO would like to thank the Department of Atomic Energy for the award of the Raja Ramanna Fellowship.

ABBREVIATIONS

CTS, Cu_3SnS_4; ATR, Attenuated Total Reflection; HER, Hydrogen Evolution Reaction.

REFERECES

(1) White, J. L.; Baruch, M. F.; Pander, J. E.; Hu, Y.; Fortmeyer, I. C.; Park, J. E.; Zhang, T.; Liao, K.; Gu, J.; Yan, Y.; Shaw T. W.; Abelev E.; Bocarsly A. B. Light-Driven Heterogeneous Reduction of Carbon Dioxide: Photocatalysts and Photoelectrodes. *Chem. Rev.* **2015**, *115* (23), 12888–12935.

(2) Marszewski, M.; Cao, S.; Yu, J.; Jaroniec, M. Semiconductor-Based Photocatalytic CO_2 Conversion. *Mater. Horizons* **2015**, *2* (3), 261–278.

(3) Di, T.; Xu, Q.; Ho, W. K.; Tang, H.; Xiang, Q.; Yu, J. Review on Metal Sulphide-Based Z-Scheme Photocatalysts. *ChemCatChem*. 2019, pp 1394–1411.

(4) Li, X.; Yu, J.; Jaroniec, M.; Chen, X. Cocatalysts for Selective Photoreduction of CO_2 into Solar Fuels. *Chem. Rev.* **2019**, *119* (6), 3962–4179.

(5) Chang, X.; Wang, T.; Gong, J. CO_2 Photo-Reduction: Insights into CO_2 Activation and Reaction on Surfaces of Photocatalysts. *Energy Environ. Sci.* **2016**, *9* (7), 2177–2196.

(6) Álvarez, A.; Borges, M.; Corral-Pérez, J. J.; Olcina, J. G.; Hu, L.; Cornu, D.; Huang, R.; Stoian, D.; Urakawa, A. CO_2 Activation over Catalytic Surfaces. *ChemPhysChem* **2017**, *18* (22), 3135–3141.

(7) Kamat, P. V. Semiconductor Surface Chemistry as Holy Grail in Photocatalysis and Photovoltaics. *Acc. Chem. Res.* **2017**, *50* (3), 527–531.

(8) Inoue, T.; Fujishima, A.; Konishi, S.; Honda, K. Photoelectrocatalytic Reduction of Carbon Dioxide in Aqueous Suspensions of Semiconductor Powders. *Nature*. 1979, pp 637–638.

(9) Liu, X.; Ye, L.; Liu, S.; Li, Y.; Ji, X. Photocatalytic Reduction of CO_2 by ZnO Micro/Nanomaterials with Different Morphologies and Ratios of {0001} Facets. *Sci. Rep.* **2016**, *6*, 1–9.

(10) Xin, C.; Hu, M.; Wang, K.; Wang, X. Significant Enhancement of Photocatalytic Reduction of CO_2 with H_2O over ZnO by the Formation of Basic Zinc Carbonate. *Langmuir* **2017**, *33* (27), 6667–6676.

(11) Li, K.; Peng, B.; Peng, T. Recent Advances in Heterogeneous Photocatalytic CO_2 Conversion to Solar Fuels. *ACS Catal.* **2016**, *6* (11), 7485–7527.

(12) Shehzad, N.; Tahir, M.; Johari, K.; Murugesan, T.; Hussain, M. A Critical Review on TiO_2 Based Photocatalytic CO_2 Reduction System: Strategies to Improve Efficiency. *J. CO_2 Util.* **2018**, *26* (November 2017), 98–122.

(13) Park, H. A.; Choi, J. H.; Choi, K. M.; Lee, D. K.; Kang, J. K. Highly Porous Gallium Oxide with a High CO_2 Affinity for the Photocatalytic Conversion of Carbon Dioxide into Methane. *J. Mater. Chem.* **2012**, *22* (12), 5304–5307.

(14) Pan, Y. X.; Liu, C. J.; Mei, D.; Ge, Q. Effects of Hydration and Oxygen Vacancy on CO_2 Adsorption and Activation on β-Ga_2O_3(100). *Langmuir* **2010**, *26* (8), 5551–5558.

(15) Yu, J.; Jin, J.; Cheng, B.; Jaroniec, M. A Noble Metal-Free Reduced Graphene Oxide-CdS Nanorod Composite for the Enhanced Visible-Light Photocatalytic Reduction of CO_2 to Solar Fuel. *J. Mater. Chem. A* **2014**, *2* (10), 3407–3416.

(16) Li, Q.; Guo, B.; Yu, J.; Ran, J.; Zhang, B.; Yan, H.; Gong, J. R. Highly Efficient Visible-Light-Driven Photocatalytic Hydrogen Production of CdS-Cluster-Decorated Graphene Nanosheets. *J. Am. Chem. Soc.* **2011**, *133* (28), 10878–10884.

(17) Jin, J.; He, T. Facile Synthesis of Bi2S3 Nanoribbons for Photocatalytic Reduction of CO_2 into CH_3OH. *Appl. Surf. Sci.* **2017**, *394*, 364–370.

(18) Zhou, R.; Guzman, M. I. CO_2 Reduction under Periodic Illumination of ZnS. *J. Phys. Chem. C* **2014**, *118* (22), 11649–11656.

(19) Manzi, A.; Simon, T.; Sonnleitner, C.; Döblinger, M.; Wyrwich, R.; Stern, O.; Stolarczyk, J. K.; Feldmann, J. Light-Induced Cation Exchange for Copper Sulfide Based CO_2 Reduction. *J. Am. Chem. Soc.* **2015**, *137* (44), 14007–14010.

(20) Sun, Y.; Li, G.; Xu, J.; Sun, Z. Visible-Light Photocatalytic Reduction of Carbon Dioxide over SnS_2. *Mater. Lett.* **2016**, *174*, 238–241.

(21) Jiao, X.; Li, X.; Jin, X.; Sun, Y.; Xu, J.; Liang, L.; Ju, H.; Zhu, J.; Pan, Y.; Yan, W.; Lin Y.; Xie Y. Partially Oxidized SnS_2 Atomic Layers Achieving Efficient Visible-Light-Driven CO_2 Reduction. *J. Am. Chem. Soc.* **2017**, *139* (49), 18044–18051.

(22) Zhu, J.; Xiao, P.; Li, H.; Carabineiro, S. A. C. Graphitic Carbon Nitride : Synthesis , Properties , and Applications in Catalysis. *ACS Appl. Mater. Interfaces* **2014**, *6*, 16449–16465.

(23) Larmier, K.; Liao, W.-C.; Tada, S.; Lam, E.; Verel, R.; Bansode, A.; Urakawa, A.; Comas-Vives, A.; Copéret, C. CO_2-to-Methanol Hydrogenation on Zirconia-Supported Copper Nanoparticles: Reaction Intermediates and the Role of the Metal-Support Interface. *Angew. Chemie Int. Ed.* **2017**, *56* (9), 2318–2323.

(24) Navalón, S.; Dhakshinamoorthy, A.; Álvaro, M.; Garcia, H. Photocatalytic CO_2 Reduction

Using Non-Itanium Metal Oxides and Sulfides. *ChemSusChem* **2013**, *6* (4), 562–577.

(25) Xu, F.; Zhang, J.; Zhu, B.; Yu, J.; Xu, J. $CuInS_2$ Sensitized TiO_2 Hybrid Nanofibers for Improved Photocatalytic CO_2 Reduction. *Appl. Catal. B Environ.* **2018**, *230* (2010), 194–202.

(26) Takayama, T.; Sato, K.; Fujimura, T.; Kojima, Y.; Iwase, A.; Kudo, A. Photocatalytic CO_2 Reduction Using Water as an Electron Donor by a Powdered Z-Scheme System Consisting of Metal Sulfide and an RGO–TiO_2 Composite. *Faraday Discuss.* **2017**, *198*, 397–407.

(27) Kamat, P. V.; Jin, S. Semiconductor Photocatalysis: " Tell Us the Complete Story! " . *ACS Energy Lett.* **2018**, *3* (3), 622–623.

(28) Liu, H.; Chen, Z.; Jin, Z.; Su, Y.; Wang, Y. A Reduced Graphene Oxide Supported Cu_3SnS_4 Composite as an Efficient Visible-Light Photocatalyst. *Dalt. Trans.* **2014**, *43* (20), 7491–7498.

(29) Lin, X.; Kavalakkatt, J.; Ennaoui, A.; Lux-Steiner, M. C. $Cu_2ZnSn(S, Se)_4$ Thin Film Absorbers Based on ZnS, SnS and Cu_3SnS_4 Nanoparticle Inks: Enhanced Solar Cells Performance by Using a Two-Step Annealing Process. *Sol. Energy Mater. Sol. Cells* **2015**, *132*, 221–229.

(30) Zhao, B.; Li, S.; Che, M.; Zhu, L. Synthesis of Cu_3SnS_4 nanoparticles with a Novel Structure as Low-Cost Counter Electrode in Dye-Sensitized Solar Cell. *Int. J. Electrochem. Sci.* **2016**, *11* (8), 6514–6522.

(31) M, T.; Sharma, N.; Das, T.; Varhade, S.; Badadhe, S. S.; Thotiyl, M. O.; Kabir, M.; Ogale, S. A Combined Experimental and Computational Study of Gas Sensing by Cu_3SnS_4 Nanoparticulate Film: High Selectivity, Stability, and Reversibility for Room Temperature H_2S Sensing. *Adv. Mater. Interfaces* **2018**, *5* (10), 1701492–1701500.

(32) Grimme, S.; Antony, J.; Ehrlich, S.; Krieg, H. A Consistent and Accurate Ab Initio Parametrization of Density Functional Dispersion Correction (DFT-D) for the 94 Elements H-Pu. *J. Chem. Phys.* **2010**, *132* (15), 154104.

(33) Grimme, S. Accurate Description of van Der Waals Complexes by Density Functional Theory Including Empirical Corrections. *J. Comput. Chem.* **2004**, *25* (12), 1463–1473.

(34) Xiong, Y.; Xie, Y.; Du, G.; Su, H. From 2D Framework to Quasi-1D Nanomaterial: Preparation, Characterization, and Formation Mechanism of Cu_3SnS_4 Nanorods. *Inorg. Chem.* **2002**, *41* (11), 2953–2959.

(35) Lin, X.; Steigert, A.; Lux-Steiner, M. C.; Ennaoui, A. One-Step Solution-Based Synthesis and Characterization of Kuramite Cu_3SnS_4 Nanocrystals. *RSC Adv.* **2012**, *2* (26), 9798.

(36) Narongrit, T.; Somchai, T.; Titipun, T. Characterization of Cu_3SnS_4 Nanoparticles and Nanostructured Flowers Synthesized by a Microwave-Refluxing Method. *Jpn. J. Appl. Phys.* **2013**, *52* (11R), 111201–111205.

(37) Blaha, P.; Schwarz, K.; Madsen, G. K. H.; Kvasnicka, D.; Luitz, J. *{WIEN2K}, {A}n {A}ugmented {P}lane {W}ave + {L}ocal {O}rbitals {P}rogram for {C}alculating {C}rystal {P}roperties*; {K}arlheinz Schwarz, Techn. Universität Wien, Austria, 2001.

(38) Slamet; Nasution, H. W.; Purnama, E.; Kosela, S.; Gunlazuardi, J. Photocatalytic Reduction of CO_2 on Copper-Doped Titania Catalysts Prepared by Improved-Impregnation Method. *Catal. Commun.* **2005**, *6* (5), 313–319.

(39) Litter, M. I. Heterogeneous Photocatalysis: Transition Metal Ions in Photocatalytic Systems. *Appl. Catal. B Environ.* **1999**, *23* (2–3), 89–114.

(40) Neatu, Ştefan; Maciá-Agullò, J. A.; Concepciòn, P.; Garcia, H. Gold-Copper Nanoalloys Supported on TiO_2 as Photocatalysts for CO_2 Reduction by Water. *J. Am. Chem. Soc.* **2014**,

136 (45), 15969–15976.

(41) Zhu, S.; Liang, S.; Bi, J.; Liu, M.; Zhou, L.; Wu, L.; Wang, X. Photocatalytic Reduction of CO_2 with H_2O to CH_4 over Ultrathin $SnNb_2O_6$ 2D Nanosheets under Visible Light Irradiation. *Green Chem.* **2016**, *18* (5), 1355–1363.

(42) Wang, Y.; Zhao, J.; Wang, T.; Li, Y.; Li, X.; Yin, J.; Wang, C. CO_2 Photoreduction with H_2O Vapor on Highly Dispersed CeO_2/TiO_2 Catalysts: Surface Species and Their Reactivity. *J. Catal.* **2016**, *337*, 293–302.

(43) Zhao, H.; Liu, L.; Andino, J. M.; Li, Y. Bicrystalline TiO_2 with Controllable Anatase-Brookite Phase Content for Enhanced CO_2 Photoreduction to Fuels. *J. Mater. Chem. A* **2013**, *1* (28), 8209–8216.

(44) Albrecht, P. M.; Jiang, D. E.; Mullins, D. R. CO_2 Adsorption as a Flat-Lying, Tridentate Carbonate on CeO_2(100). *J. Phys. Chem. C* **2014**, *118* (17), 9042–9050.

(45) Liu, L.; Zhao, C.; Miller, J. T.; Li, Y. Mechanistic Study of CO_2 Photoreduction with H_2O on Cu/TiO_2 Nanocomposites by in Situ x-Ray Absorption and Infrared Spectroscopies. *J. Phys. Chem. C* **2017**, *121* (1), 490–499.

(46) Liu, D.; Fernández, Y.; Ola, O.; MacKintosh, S.; Maroto-Valer, M.; Parlett, C. M. A.; Lee, A. F.; Wu, J. C. S. On the Impact of Cu Dispersion on CO_2 Photoreduction over Cu/TiO_2. *Catal. Commun.* **2012**, *25*, 78–82.

(47) Di, T.; Zhu, B.; Cheng, B.; Yu, J.; Xu, J. A Direct Z-Scheme g-C_3N_4/SnS_2 Photocatalyst with Superior Visible-Light CO_2 Reduction Performance. *J. Catal.* **2017**, *352*, 532–541.

(48) Wang, J.; Li, G.; Li, Z.; Tang, C.; Feng, Z.; An, H.; Liu, H.; Liu, T.; Li, C. A Highly Selective and Stable ZnO-ZrO_2 Solid Solution Catalyst for CO_2 Hydrogenation to Methanol. *Sci. Adv.* **2017**, *3* (10), e1701290–e1701300.

(49) Wang, G. W.; Hattori, H. Reaction of Adsorbed Carbon Monoxide with Hydrogen on Magnesium Oxide. *J. Chem. Soc. Faraday Trans. 1 Phys. Chem. Condens. Phases* **1984**, *80* (5), 1039–1047.

(50) Teramura, K.; Tanaka, T.; Ishikawa, H.; Kohno, Y.; Funabiki, T. Photocatalytic Reduction of CO_2 to CO in the Presence of H_2 or CH_4 as a Reductant over MgO. *J. Phys. Chem. B* **2004**, *108* (1), 346–354.

(51) Ji, Y.; Luo, Y. Theoretical Study on the Mechanism of Photoreduction of CO_2 to CH_4 on the Anatase TiO_2(101) Surface. *ACS Catal.* **2016**, *6* (3), 2018–2025.

(52) He, H.; Zapol, P.; Curtiss, L. A. Computational Screening of Dopants for Photocatalytic Two-Electron Reduction of CO_2 on Anatase (101) Surfaces. *Energy Environ. Sci.* **2012**, *5* (3), 6196–6205.

(53) An, X.; Li, K.; Tang, J. Cu_2O/Reduced Graphene Oxide Composites for the Photocatalytic Conversion of CO_2. *ChemSusChem* **2014**, *7* (4), 1086–1093.

(54) Kuehnel, M. F.; Orchard, K. L.; Dalle, K. E.; Reisner, E. Selective Photocatalytic CO_2 Reduction in Water through Anchoring of a Molecular Ni Catalyst on CdS Nanocrystals. *J. Am. Chem. Soc.* **2017**, *139* (21), 7217–7223.

(55) Jin, J.; Yu, J.; Guo, D.; Cui, C.; Ho, W. A Hierarchical Z-Scheme CdS-WO_3 Photocatalyst with Enhanced CO_2 Reduction Activity. *Small* **2015**, *11* (39), 5262–5271.

(56) Kanemoto, M.; Ishihara, K.; Wada, Y.; Sakata, T.; Mori, H.; Yanagida, S. Visible-Light Induced Effective Photoreduction of CO_2 to CO Catalyzed by Colloidal CdS Microcrystallites. *Chemistry Letters*. 1992, pp 835–836.

(57) Zhang, Y. J.; Sethuraman, V.; Michalsky, R.; Peterson, A. A. Competition between CO_2 Reduction and H2 Evolution on Transition-Metal Electrocatalysts. *ACS Catal.* **2014**, *4* (10),

3742–3748.

(58) Wu, J.; Huang, Y.; Ye, W.; Li, Y. CO_2 Reduction: From the Electrochemical to Photochemical Approach. *Adv. Sci.* **2017**, *4* (11), 1–29.

Figures

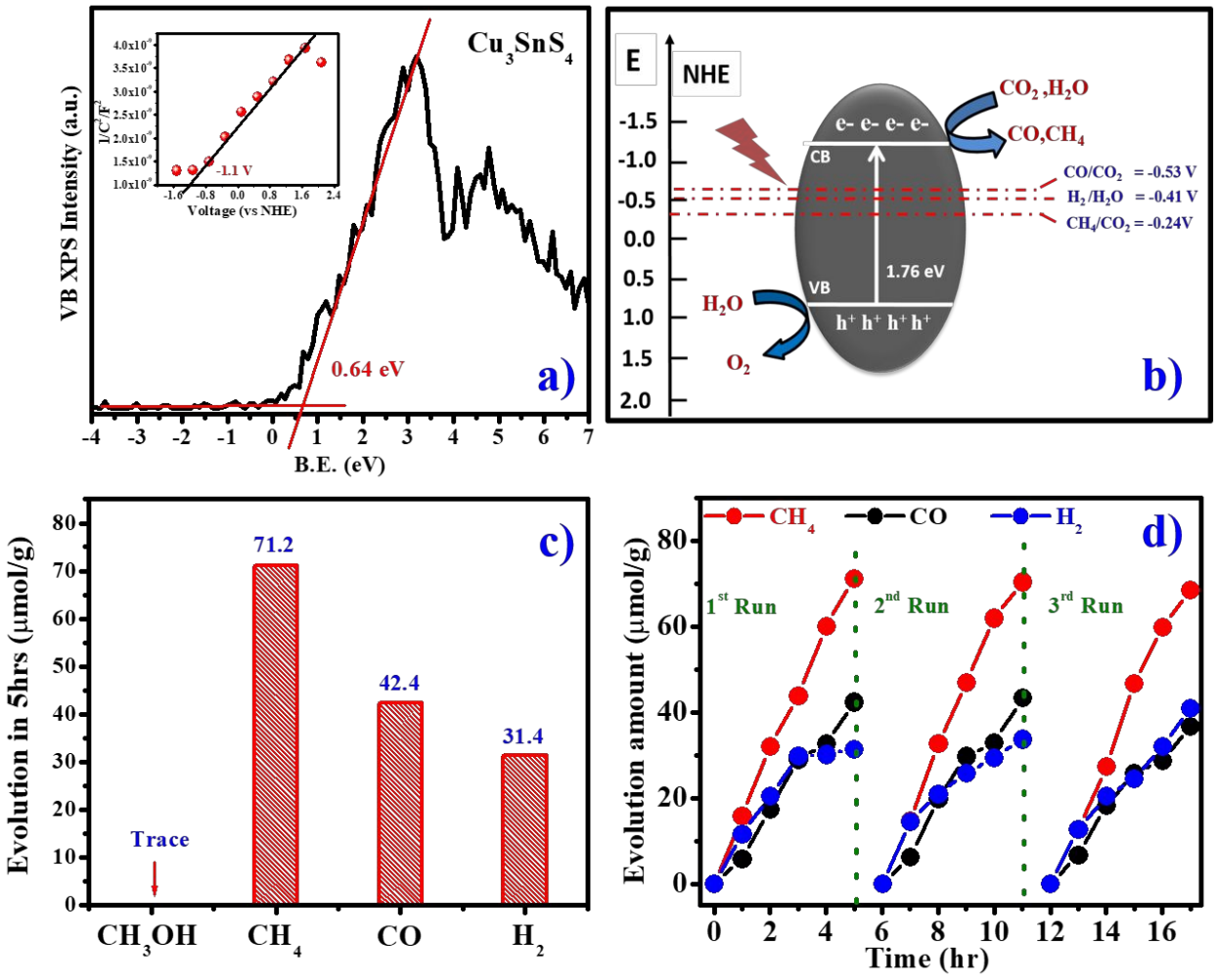

Figure 1. a) Valence Band spectra with Mott Schottky plot in inset. **b)** Energy level diagram. **c)** Evolved reduced products after photocatalytic CO_2 reduction over CTS sample. **d)** Stability profile of CTS.

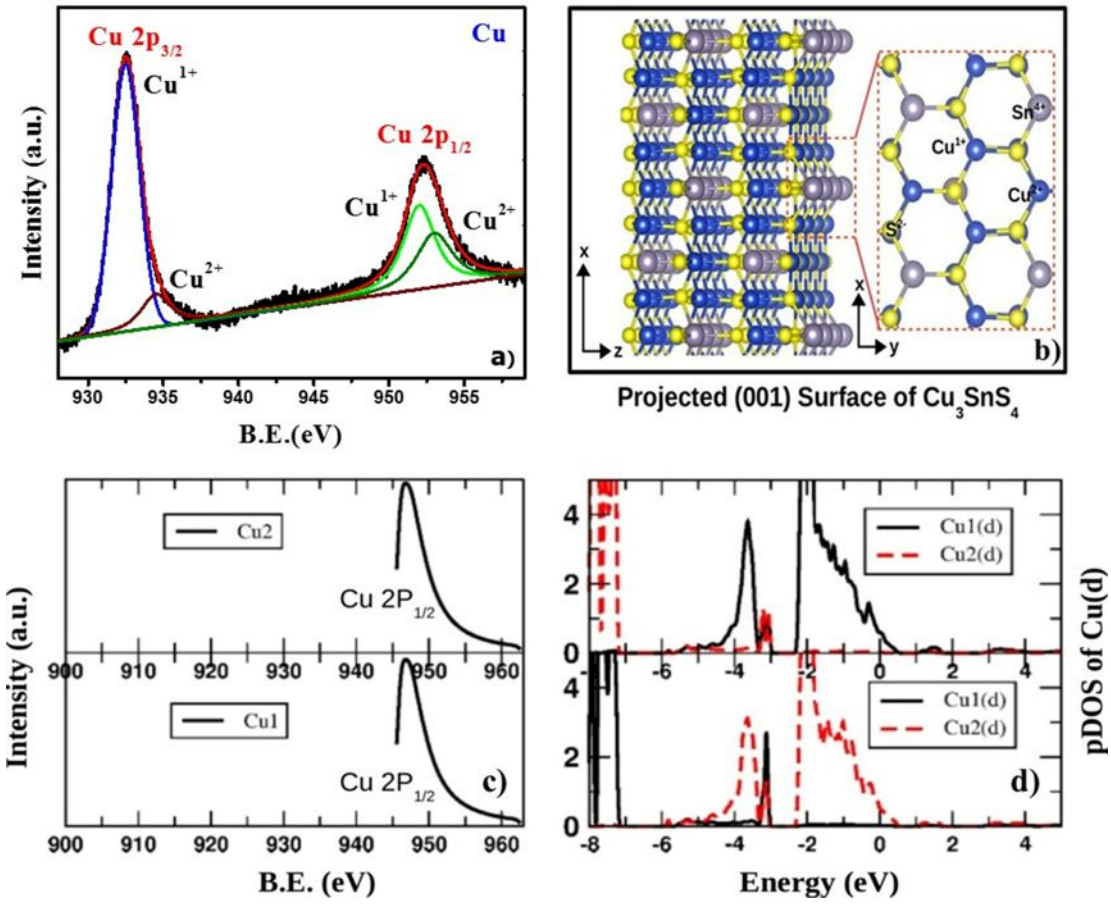

Figure 2. a) XPS spectra of Copper (Cu) over CTS surface. **b)** The optimized four layers slab of CTS grown along <001> which is projected with top most layer exposed upward, with grey balls for Sn, Blue for Cu and yellow for S atoms **c)** The calculated L_2 edges of Cu^{1+} and Cu^{2+} **d)** Projected density of states (p DOS) from Cu-*d* of the same Cu1 and Cu2 atoms.

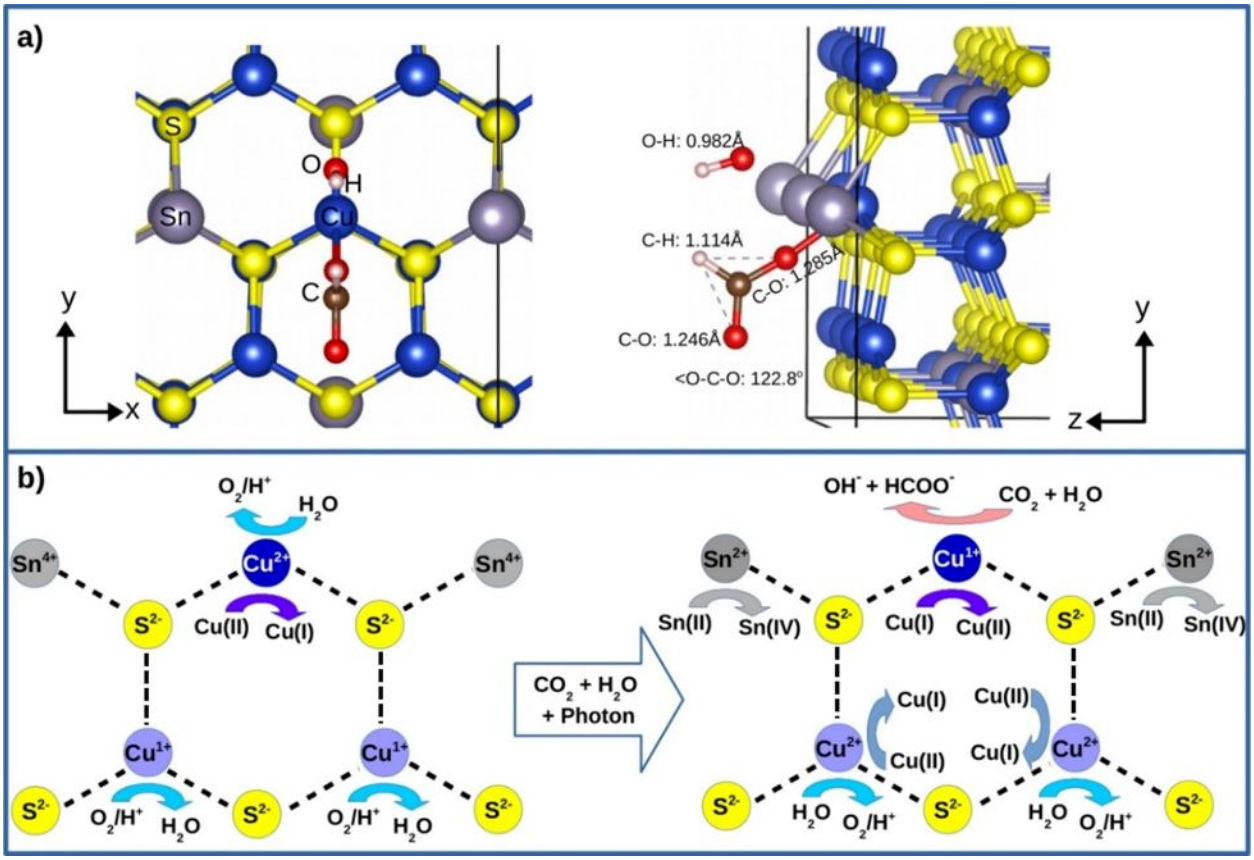

Figure 3. In panel **a)**, the optimized geometry of the CTS NPs (001) surface with Cu-Sn termination is exposed to the best-suited CO_2 and H_2O gases and possible formation of formate is shown. In panel **b)**, the schematic representation of the CO_2 activation via valence state change of cations of CTS (001) surface viable for the formate route.

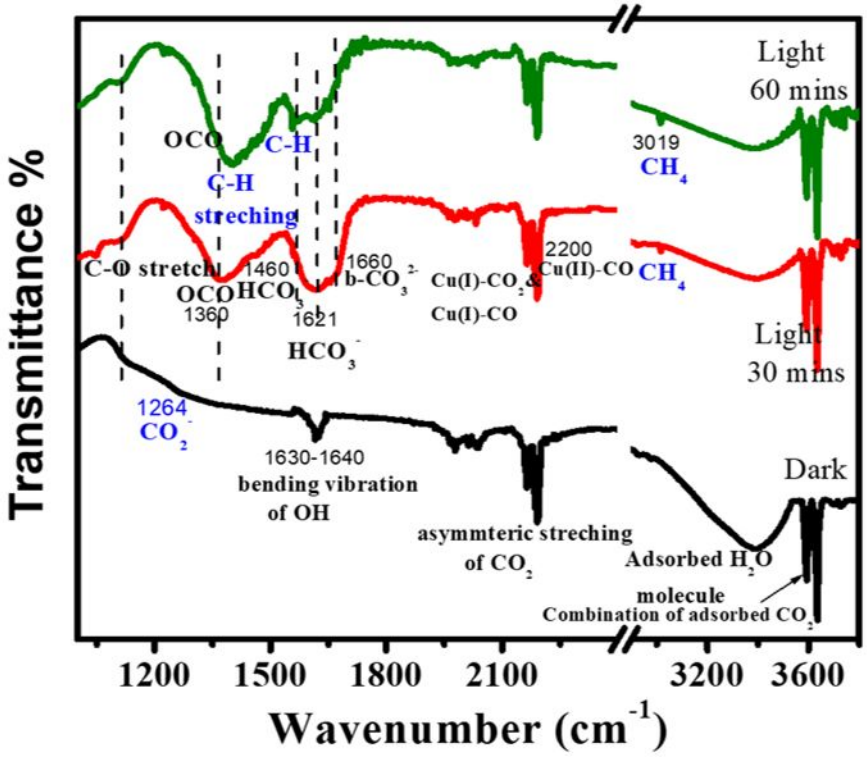

Figure 4. *In situ* Attenuated Total Reflection (ATR) of CTS in presence of purged CO_2 and water vapour.

TOC ENTRY

Experimental and theoretical investigation of Cu-Sn terminated surface of Cu_3SnS_4 for selective photocatalytic CO_2 reduction to CH_4.

TOC GRAPHIC